doi.org/10.1002/cbdv.202400267 Review CHEMISTRY & BIODIVERSITY

www.cb.wiley.com

Nα-Aroyl-*N*-Aryl-Phenylalanine Amides: A Promising Class of Antimycobacterial Agents Targeting the RNA Polymerase

Rüdiger W. Seidel,*[a] Richard Goddard,[b] Markus Lang,[a] and Adrian Richter[a]

Dedicated to Professor Michael Spiteller on the occasion of his 70th birthday

Tuberculosis (TB), caused by *Mycobacterium tuberculosis*, remains the leading cause of death from a bacterium in the world. The global prevalence of clinically relevant infections with opportunistically pathogenic non-tuberculous mycobacteria (NTM) has also been on the rise. Pharmacological treatment of both TB and NTM infections usually requires prolonged regimens of drug combinations, and is often challenging because of developed or inherent resistance to common antibiotic drugs. Medicinal chemistry efforts are thus needed to improve treatment options and therapeutic outcomes. *Nα*-aroyl-*N*-aryl-phenylalanine amides (AAPs) have been identified as potent antimycobacterial agents that target the RNA polymerase with a low probability of cross resistance to rifamycins, the clinically most important class of antibiotics known to inhibit the bacterial RNA polymerase. In this review, we describe recent developments in the field of AAPs, including synthesis, structural characterization, *in vitro* microbiological profiling, structure-activity relationships, physicochemical properties, pharmacokinetics and early cytotoxicity assessment.

1. Introduction

Mycobacterial infections constitute a global public health issue. These infections can be classified as two types, viz. tuberculosis (TB) and those caused by non-tuberculous mycobacteria (NTM). TB continues to be the most lethal infectious disease caused by a bacterium. According to the WHO, there was an estimate of 1.13 million TB deaths among HIV-negative people and an estimated number of 167.000 deaths among people living with HIV worldwide in 2022.[1] The etiological agent of TB is *Mycobacterium tuberculosis*, a slowly dividing mycobacterium. TB primarily manifests as lung disease (pulmonary TB) but can also affect other organs and tissue (extrapulmonary TB).[2] NTM, encompassing mycobacteria causing neither TB nor leprosy, are also increasingly identified as opportunistic pathogens.[3] NTM infections likewise predominantly manifest themselves as pulmonary disease (NTM-PD), resembling pulmonary TB. Patients with structural lung diseases such as cystic fibrosis,[4] bronchiectasis,[5] chronic obstructive pulmonary disease and a history of pulmonary TB are at particular risk of developing NTM-PD.[6] Since most countries in the world do not have surveillance systems for NTM-PD, the epidemiological burden of the disease is more difficult to estimate than for TB.[7] *Mycobacterium abscessus*[8] and the *Mycobacterium avium* complex (MAC)[8e] are among the clinically most relevant species causing NTM-PD. Similar to *M. tuberculosis*, opportunistically pathogenic NTM can also lead to less common extrapulmonary diseases, such as cervical lymphadenitis in children,[9] skin and soft tissue infections[10] and disseminated disease in patients with compromised immune systems.[11]

Although advances have been made recently, treatment of TB[12] and NTM infections[13] still requires multidrug regimens of several months, because the pathogens occupy various infection niches with diverse microenvironments.[14] Monotherapies can also accelerate the development of drug resistance.[15] Rifamycins are a class of antibiotics that are particularly effective against mycobacteria. Their antibacterial activity relies on inhibition of the bacterial transcription through allosteric binding to the DNA-dependent RNA polymerase (RNAP) leading to cell death.[16] The semi-synthetic rifampicin (also known as rifampin) of the rifamycin family is a first-line anti-TB drug.[17] Due to its exceptional sterilizing capability, it remains an indispensable drug against drug-susceptible TB, even more than 50 years after its introduction.[18] Nevertheless, *M. tuberculosis* strains resistant to rifampicin have become a particular threat.[19] Cross-resistance between rifampicin and other semi-synthetic rifamycin analogs, such as rifabutin and rifapentine, which has been encountered in *M. tuberculosis* isolates,[20] renders these analogs less promising as substitutes for rifampicin in the therapy of drug-resistant TB. Rifampicin-based regimens have particularly been recommended for the treatment of the less common NTM-PD.[21] Although rifamycins have been included in three-drug regimens to treat pulmonary MAC infections, their role appears to be unclear.[21a,22] Rifabutin exhibits bactericidal activity against *M. abscessus in vitro*[23] and is being investigated in a clinical study to treat *M. abscessus*

[a] Dr. R. W. Seidel, M. Lang, Dr. A. Richter
Institut für Pharmazie, Martin-Luther-Universität Halle-Wittenberg, Wolfgang-Langenbeck-Str. 4, 06120 Halle (Saale), Germany
E-mail: ruediger.seidel@pharmazie.uni-halle.de

[b] Dr. R. Goddard
Max-Planck-Institut für Kohlenforschung, Kaiser-Wilhelm-Platz 1, 45470 Mülheim an der Ruhr, Germany

pulmonary disease.[24] Rifampicin and rifapentine are not active against *M. abscessus* because of the pathogen's intrinsic resistance.[25] New RNAP inhibitors without cross-resistance to rifamycins are thus required as new therapeutic options for TB and NTM infections.

*N*α-aroyl-*N*-aryl-phenylalanine amides (AAPs) have been identified as a promising class of antimycobacterial agents that selectively target the mycobacterial RNAP with a low probability of cross-resistance to rifamycins. GlaxoSmithKline (GSK) first discovered antimycobacterial activity of *N*α-2-thiophenoyl-D-phenylalanine-2-morpholinoanilide (**1**) in a phenotypic high-throughput screening of an in-house compound library.[26] We and others found *R*-**1** (Figure 1) as a hit compound in whole cell screenings of the Pathogen Box® library, provided by Medicines for Malaria Ventures (MMV, Geneva, Switzerland) against *M. abscessus*[27] and *M. avium*.[27a] Ebright and colleagues identified the compound class as potent, selective and stereospecific inhibitors of the mycobacterial RNAP in a screening of a compound library by using an enzyme inhibition assay.[28] Figure 1 shows their prototypical compound named **D-AAP1**.[28a] Compound *R*-**1** and **D-AAP1** served as starting points for microbiological profiling and lead optimization. Herein, we give an account of recent developments in the field of AAPs, including synthesis, structural and biological characterization, structure-activity relationship (SAR), physicochemical and pharmacokinetic properties and early cytotoxicity assessment.

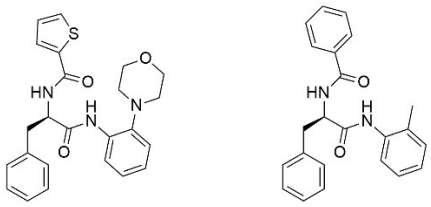

R-**1** **D-AAP1**

Figure 1. Chemical diagrams of *R*-**1** (contained in the Pathogen Box® library as MMV688845) and **D-AAP1**.[28a]

2. Chemistry

2.1. Amide Bond Formation

AAPs can be thought of as modular structures comprising two aromatic moieties attached to the amino and the carboxy group of phenylalanine through amide bonds (Figure 1). This feature facilitates structural variation via amide coupling reactions using commercially available building blocks. Various methods for the synthesis of AAPs, utilizing *N*-protected α-amino acids as starting materials and different coupling reagents known from peptide synthesis,[29] have been described. Ebright and colleagues reported the preparation of the prototypical **D-AAP1** and a large variety of derivatives.[28a,30] The racemate **DL-AAP1**

Rüdiger W. Seidel graduated in chemistry from the Heinrich-Heine-Universität Düsseldorf, Germany, in 2006. He then joined the research group of Iris M. Oppel at the Ruhr-Universität Bochum, Germany, where he finished his PhD thesis in the field of solid-state supramolecular chemistry in 2010. In 2010/2011, he did a postdoctoral stay with Christian W. Lehmann at the Max-Planck-Institut für Kohlenforschung in Mülheim an der Ruhr, Germany. In 2019, he completed his studies in pharmacy at the Martin-Luther-Universität Halle-Wittenberg, Halle (Saale), Germany, where he is presently a postdoctoral researcher in the group of Peter Imming. His current research interest is characterization of new antimycobacterial agents.

Richard Goddard obtained a BSc (1973) and a PhD (1977) in chemistry from the University of Bristol, UK. In 1976, he joined the chemical crystallography group, led by Carl Krüger, at the Max-Planck-Institut (MPI) für Kohlenforschung in Mülheim an der Ruhr, Germany. In 1979, he moved to Cornell University, Ithaca, USA, for a one-year research stay with Roald Hoffmann, where he worked on agostic interactions. Thereafter, he was a staff scientist at the MPI für Kohlenforschung in the Department of Chemical Crystallography and Electron Microscopy until 2017, and has been a guest scientist there since then. His research interests include X-ray crystallography, crystal growth and quantum crystallography.

Markus Lang studied pharmacy at the Martin-Luther-Universität Halle-Wittenberg (MLU) in Halle (Saale), Germany, from 2013 to 2017. He then did his diploma thesis at MLU under the supervision of Lea-Ann Dailey. In 2019, he joined the research group of Peter Imming at MLU as a PhD student. The focus of his thesis work is the synthesis and characterization of antimycobacterial phenylalanine amides. During the summer of 2023, he spent two months in the research group of Thomas Dick at the Center of Discovery and Innovation in Nutley, New Jersey, USA, where he conducted in vitro susceptibility testing against non-tuberculous mycobacteria.

Adrian Richter completed his studies in pharmacy at the Martin-Luther-Universität Halle-Wittenberg (MLU) in Halle (Saale), Germany, in 2011. In 2013, he joined the group of Peter Imming at MLU for his PhD thesis on antitubercular benzothiazinones, which he defended in 2017. He then did a postdoctoral stay in Yossef Av-Gay's group at the University of British Columbia in Vancouver, Canada, focussing on in vitro testing against intracellular M. tuberculosis and M. abscessus. In 2019, he returned to the MLU in order to work towards his Habilitation. His current research interests concentrate on antimycobacterial drug discovery, with emphasis on M. abscessus.

was prepared from commercially available benzoyl-DL-phenylalanine and *o*-toluidine with the aid of polymer-bound carbodiimide and hydroxybenzotriazole (HOBt) as coupling reagents. Since AAPs are stereospecific RNAP inhibitors (Section 3.3), isolation of the enantiomerically pure compounds is particularly desirable. As shown in Scheme 1, using enantiopure benzoyl-D-phenylalanine (**2**) as starting material under the same reaction conditions resulted in 10% *ee* of **D-AAP1**. In turn, starting from benzoyl-L-phenylalanine afforded 10% *ee* of **L-AAP1**. The enantiomers were then separated by chiral chromatography. A second method mentioned by the same authors utilized phosphorous oxychloride[31] as coupling reagent in anhydrous pyridine and in the presence of imidazole.[30]

For the *N*α-selenophenoyl analogue of **D-AAP1**, named **D-IX336**, Ebright and co-workers reported a racemization-free synthesis starting from Fmoc-D-phenylalanine (**3**, Scheme 2).[28a] The carboxy group is activated with oxalyl chloride, and the formation of the first amide bond is achieved by subsequent reaction with *o*-toluidine, affording the Fmoc-*N*-(*o*-tolyl)-D-phenylalanine amide **4**. After removal of Fmoc with piperidine, reaction with selenophene-2-carboxylic acid using T3P® (propanephosphonic acid anhydride)[32] as coupling reagent in the presence of *N*,*N*-diisopropylethylamine (DIPEA, also known as Hünig's base) affords **D-IX336**. 100% *ee* was reported for both reaction steps. The T3P® coupling reagent is known for its ability to result in a low degree of racemization of racemization-prone carboxylic acid substrates.[33]

Recently, we established a two-step synthetic route to the screening hit *R*-**1** (Section 3.1), which avoids racemization.[34] We conceived two pathways for this purpose. As outlined in Scheme 3, racemization-free synthesis of *R*-**1** was achieved by reaction of Boc-D-phenylalanine (**5**) with 2-morpholinoaniline using T3P® as coupling reagent in a mixture of ethyl acetate and pyridine at 0° C, resulting in the formation of Boc-D-phenylalanine-2-morpholino-anilide (**6**). After removal of the protecting group, the 2-thiophenoyl group was introduced by reaction with 2-thiophenecarboxylic acid and the PyBOP® coupling reagent[35] in the presence of DIPEA. Virtually no racemization occurred, as revealed by chiral HPLC (99.9% *ee*). By analogy, the enantiomer *S*-**1** could be obtained with 99.9% *ee* from Boc-L-phenylalanine. Although a different *N*-protecting group and different coupling reagent in each step were utilized, the synthetic approach, *viz.* coupling of the carboxy group with an arylamine in the first step and coupling of the amino group with an arenecarboxylic acid in the second, is closely related to the synthesis of **D-IX336** by Ebright and colleagues[28a] (Scheme 2).

The second pathway that we explored started from unprotected D-phenylalanine (**7**).[34] As shown in Scheme 4, compound **7** was first reacted with 2-thiophenecarbonyl chloride to yield the *N*α-thiophenoyl-D-phenylalanine **8**, which was then reacted with 2-morpholinoaniline in the presence of PyBOP® and DIPEA in dichloromethane. Stereochemical evaluation of the pathway revealed that the racemization appears to occur almost exclusively in the amide coupling of the amino acid carboxy group, *i.e.* in the second step, since compound **8** exhibited 99.1% *ee*. The formation of *rac*-**1** was initially revealed by X-ray crystallography of a crystal of the product (Section 2.3) and subsequently confirmed by chiral HPLC and determination of the specific rotation of the bulk material. Analogously, starting from L-phenylalanine also resulted in virtually complete racemization in the second step. It is known that *N*-acyl amino acids like in **8** are more prone to racemization than carbamates, *viz.* Fmoc- or Boc-protected amino acids such as **4** and **6**, which can be rationalized in terms of the higher NH acidity of *N*-acyl amino acids than carbamates.[36] Moreover, the formation of a

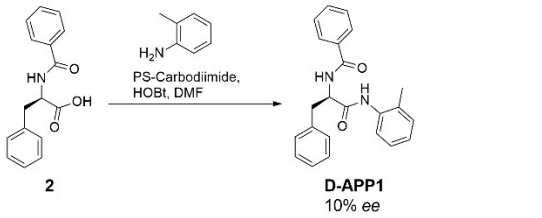

Scheme 1. Synthesis of **D-AAP1** from benzoyl-D-phenylalanine (**2**). PS-Carbodiimide: polymer-bound carbodiimide; HOBt: hydroxybenzotriazole.

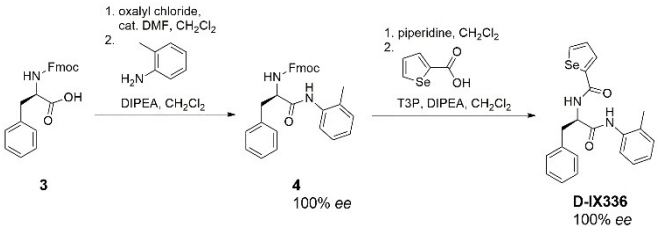

Scheme 2. Racemization-free synthesis of **D-IX336** from Fmoc-D-phenylalanine (**3**). Fmoc: fluorenylmethoxycarbonyl; T3P: propanephosphonic acid anhydride.

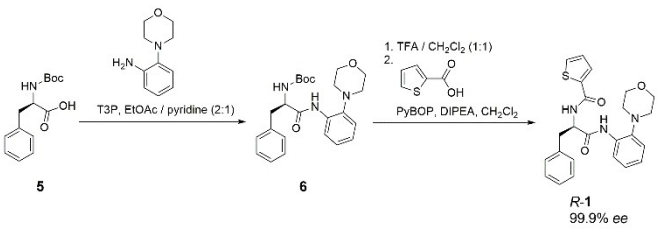

Scheme 3. Racemization-free synthesis of *R*-**1** from Boc-D-phenylalanine (**5**). Boc: *tert*-butyloxycarbonyl; T3P: propanephosphonic acid anhydride; PyBOP: benzotriazol-1-yloxytripyrrolidinophosphonium hexafluorophosphate.

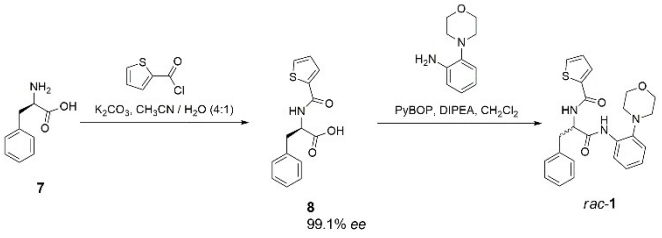

Scheme 4. Two-step synthesis of **1** from D-phenylalanine (**7**), resulting in complete racemization. PyBOP: benzotriazol-1-yloxytripyrrolidinophosphonium hexafluorophosphate.

hydroxy-benzotriazole ester upon activation of the carboxy group with PyBOP® increases the electron-withdrawing effect on the α-carbon atom and thus likely accounts for the observed racemization. Enolization or oxazolone formation can be considered as possible mechanisms.[37]

Eventually, we opted for the two-step method sketched in Scheme 3 for the synthesis of a variety of analogues of the hit compound *R*-**1** for investigating structure activity relationships (SAR) and hit-to-lead optimization (Section 4), as summarized in Scheme 5.[38] Thus, an aniline building block is coupled to the carboxy group of a Boc-protected aromatic α-amino acid **9** to give the anilide **10**. In general, **10** is obtained in good yields in this step,[38–39] but introduction of a methyl group in *ortho* position on the aniline moiety or on the aniline nitrogen atom (Section 2.2) appears to decrease the yields considerably owing to steric hindrance.[39] In the second step, aroylation of the α-amino group after Boc removal yields the *N*α-aroyl-amino acid anilide **11**. *N*α-methyl *R*-**1** was obtained by starting from commercially available Boc-*N*-methyl-D-phenylalanine.[39] Likewise, steric hindrance of the α-amino group and the aryl benzoic acids to be coupled seems to lower the yields.

Occasionally, we replaced PyBOP® by 3-(diethoxy-phosphoryloxy)-1,2,3-benzotriazin-4(3H)-one (DEPBT) as coupling reagent in the second step shown in Scheme 5.[40] In general, both seem to work equally well for the purpose, except for amide coupling of the sterically hindered 2,6-dimethylbenzoic acid for which DEPBT proved unsuitable.[39] DEPBT has the advantage of forming highly polar by-products (diethylphosphate), which constitutes an advantage for chromatographic work-up of polar products. Using PyBOP®, in contrast, results in a less polar phosphoric acid triamide by-product, which proved beneficial for chromatographic purification of less polar products. By way of example, we showed by chiral HPLC that virtually no racemization took place in the synthesis of *R*-**1** from Boc-D-phenylalanine (and likewise for *S*-**1** from Boc-L-phenylalanine) using DEPBT as coupling reagent in the second amide bond formation step.[38]

2.2. Aniline Building Blocks

Variation of the 2-morpholinoaniline moiety in the hit compound *R*-**1** is crucial for comprehensive SAR studies and successful hit-to-lead optimization. Since postsynthetic chemical alteration of this moiety might result in unintended changes to other parts of the target AAP, a synthetic route in which the aniline building block is modified prior to amide coupling is preferred. Replacement of the morpholine ring by thiomorpholine was achieved by a solvent-free nucleophilic aromatic substitution reaction (Scheme 6).[38] Heating 1-bromo-2-nitrobenzene **12** to 120 °C in pure thiomorpholine gave the 4-(2-nitrophenyl)thiomorpholine **13**. Subsequent reduction of the nitro group with aqueous hydrazine in ethanol using Pd/C as catalyst[41] resulted in the desired 2-thiomorpholinoaniline **14**. H_2 and $Pd(OH)_2$/C in ethanol also proved suitable for reduction of nitroaromatic precursors to the desired aniline building blocks.[39] A microwave-assisted synthesis of **13** from 1-fluoro-2-nitrobenzene and thiomorpholine in the presence of triethylamine in dioxane (160 °C, 15 min), and subsequent reduction to **14** with H_2 on Pd/C has been disclosed.[42] Of note, the synthesis of 4-(2-nitrophenyl)morpholine and **13** via decarboxylative *ipso* amination of the corresponding electron-deficient benzoic acid has also been reported.[43]

Attempts to react commercially available thiomorpholine 1,1-dioxide in a nucleophilic aromatic substitution in analogy to the first step shown in Scheme 6 have been unsuccessful,[38] except for the highly electron-deficient 1,3-difluoro-2-nitrobenzene.[39] We assume that the electron-withdrawing effect of the oxido groups decreases the nucleophilicity of the nitrogen atom. The nucleophilic aromatic substitution can be replaced by a Buchwald-Hartwig amination[44] in this case (Scheme 7), followed by reduction of the nitro group applying the same method as for the reduction of **13** to **14**, *i.e.* treatment of **16** with aqueous hydrazine in the presence of Pd/C in ethanol, to yield **17**. Although Buchwald-Hartwig amination proved to be suitable for the synthesis of **16**, *S*-oxidation of **13**

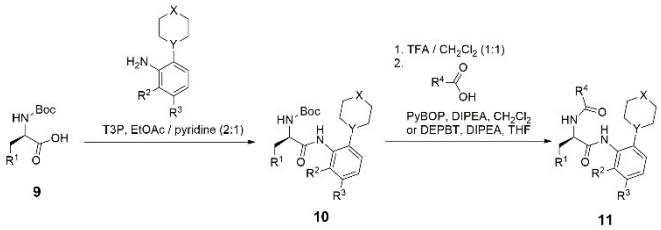

Scheme 5. General method for racemization-free synthesis of *R*-**1** derivatives **11** from Boc-D-aromatic amino acids **9**. R^1 = phenyl, *p*-hydroxyphenyl, 2- or 3- thiophenyl; R^2 = H, CH_3, F; R^3 = H, F; R^4 = 2-thiophenyl, 2-fluorophenyl; X = O, S, SO, SO_2; Y = N, CH. Boc: *tert*-butyloxycarbonyl; T3P: propanephosphonic acid anhydride; TFA: trifluoroacetic acid; PyBOP: benzotriazol-1-yloxytripyrrolidinophosphonium hexafluorophosphate.

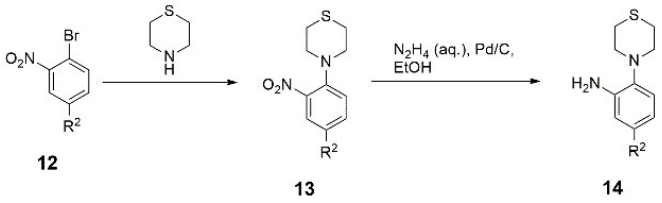

Scheme 6. Two-step preparation of 2-thiomorpholinoaniline building blocks **14** from 1-bromo-2-nitrobenzene **12** for the synthesis of *R*-**1** derivatives **11**, as shown in Scheme 5. R^2 = H, F.

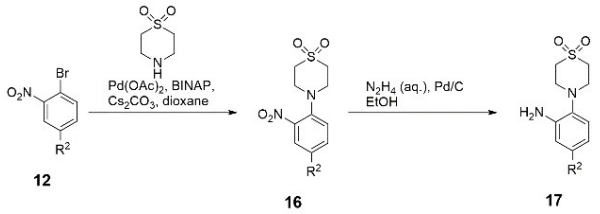

Scheme 7. Two-step preparation of 4-(2-aminophenyl)thiomorpholine 1,1-dioxide building blocks **17** from 1-bromo-2-nitrobenzene **14** for the synthesis of *R*-**1** derivatives **11**, as shown in Scheme 5. R^2 = H, F. BINAP: 2,2-bis(diphenylphosphino)-1,1-binaphthyl.

turned out to be more efficient with regard to experimental procedure, reaction yields and avoidance of palladium as a catalyst in the C–N bond formation step. Furthermore, it also facilitates the synthesis of the corresponding sulfoxide **18**, after applying the appropriate oxidizing agent and reaction conditions.[38] As shown in Scheme 8, treatment of **13** with $NaIO_4$ yields the sulfoxide **18**, whereas treatment with *m*-chloroperbenzoic acid (*m*-CPBA) affords the sulfone **16**. The increased polarity resulting from *S*-oxidation at this stage may hamper purification of consecutive products by normal phase column chromatography. Alternatively, *S*-oxidation using $NaIO_4$ or *m*-CPBA can be conducted at the stage of the Boc-protected anilide **10** when X = S (Scheme 5).[38] Oxidation reactions at the stage of compound **11** are less suitable because of possible side reactions such as *S*-oxidation of the thiophene moiety.[45]

In order to replace the thiomorpholine nitrogen atom in **14** by a CH group, a previously reported method for metal-free carbon-carbon coupling reactions of saturated heterocyclic sulfonyl-hydrazones with boronic acids was adapted.[46] Accordingly, the preparation of the 2-(tetrahydro-2*H*-thiopyran-4-yl)aniline building block **21** was carried out in two-steps (Scheme 9).[38] The heterocyclic ketone 4-oxothiane (**19**) was first reacted with tosylhydrazone to yield the sulfonylhydrazide **20**, which was subsequently coupled with Boc-protected (2-aminophenyl)boronic acid pinacol ester. Removal of the Boc protecting group finally afforded the target compound **21**.

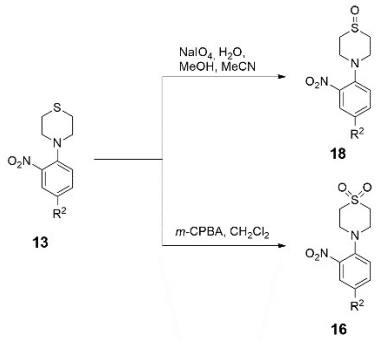

Scheme 8. Formation of the corresponding sulfoxide **18** and sulfone **16** from the 4-(2-nitrophenyl)thiomorpholine **13** through *S*-oxidation. *m*-CPBA: *m*-chloroper-benzoic acid. R^2 = H, F.

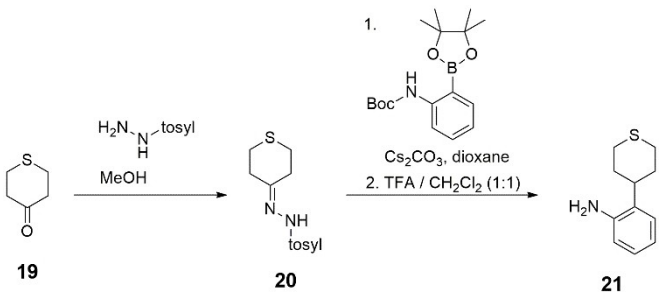

Scheme 9. Synthesis of the 2-(tetrahydro-2*H*-thiopyran-4-yl)aniline building block **21** from 4-oxothiane (**19**). tosyl: $–SO_2–C_6H_4–CH_3$; Boc: *tert*-butyloxy-carbonyl; TFA: trifluoroacetic acid.

For AAPs containing a methyl group at the anilide nitrogen atom, *N*-methyl-2-morpholinoaniline (**24**) was employed as a building block.[39] Compound **24** was prepared from 2-morpholinoaniline (**22**) via the corresponding formamide **23**, which was treated with $LiAlH_4$ (Scheme 10).[39] *N*-Heterocyclic carbene copper(I) catalyzed *N*-methylation of **22** to obtain **24**, using CO_2 and $PhSiH_3$ as reagents, has also been described in the literature.[47]

2.3. Structures of AAPs

As of January 2024, the number of structurally characterized AAPs available in the Cambridge Structural Database (CSD)[48] is rather limited.[34,38,49] To our knowledge, neither **D-AAP1** nor its derivatives have so far been characterized by small-molecule X-ray crystallography. Recently, we reported the crystal and molecular structure of *rac*-**1** (Figure 2).[34] The compound crystallizes solvent-free in the monoclinic system (centrosymmetric space group $P2_1/n$, $Z = 4$). Both amide groups exhibit a *Z* conformation with a slight out-of-plane deformation. The anilide nitrogen atom (N1) acts as a hydrogen bond donor towards the thiophenoyl oxygen atom (O2), resulting in a seven-membered intramolecular N–H···O hydrogen bond ring. Such is also encountered in the crystal structure of *N*α-benzoyl-*N*-quinolin-8-yl-phenylalanine amide (CSD refcode: SAQTEN).[49] In *rac*-**1**, two heterochiral molecules form a centrosymmetric dimer through N–H···O hydrogen bonds between the phenylalanine amide α-nitrogen atom (N2) and the amide oxygen

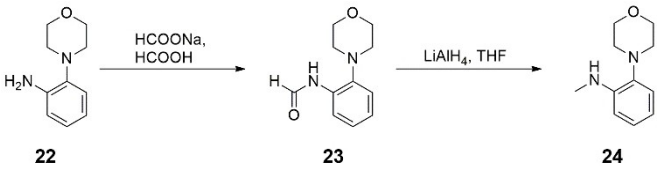

Scheme 10. Synthesis of the *N*-methyl-2-morpholinoaniline building block **24** from 2-morpholinoaniline (**22**) via *N*-(2-morpholinophenyl)formamide (**23**).

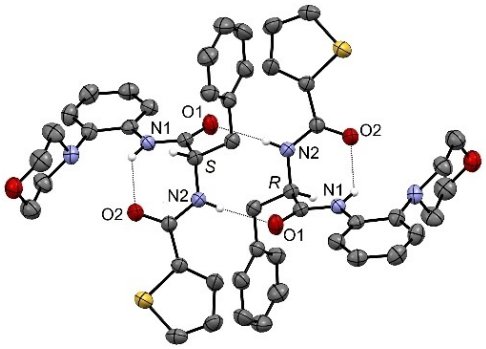

Figure 2. Centrosymmetric dimer in the crystal structure of *rac*-**1** (Figure 1; CSD refcode: BALNUB).[34] Displacement ellipsoids are drawn at the 50% probability level. Carbon-bound H atoms except at the chirality centers are omitted for clarity. Dashed lines represent hydrogen bonds. Color scheme: C, grey; H, white; N, blue; O, red, S, yellow.

atom (O1) of the symmetry-related molecule. The graph set descriptor is $R_2^2(10)$.[50]

Whereas attempts to grow crystals of enantiopure *R*-**1** suitable for X-ray diffraction analysis by the slow-evaporation method using several solvents resulted in glassy materials,[34] the enantiopure *R*-configured 2-thiomorpholinoanilide analogue **25** (Figure 3) afforded crystals and could be structurally characterized by X-ray crystallography.[38] Compound **25** crystallizes in the triclinic system (space group *P*1, *Z* = 2) with two crystallographically unique molecules (Figure 4). The molecular conformation and the intra- and intermolecular N–H···O hydrogen bond motifs found in the crystal structure of *rac*-**1** are also

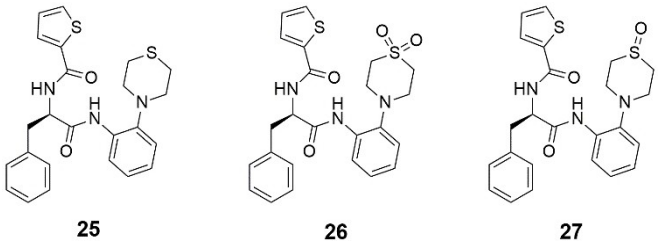

Figure 3. Chemical diagrams of the *R*-configured 2-thiomorpholinoanilide **25** and the corresponding sulfone **26** and sulfoxide **27**.[38]

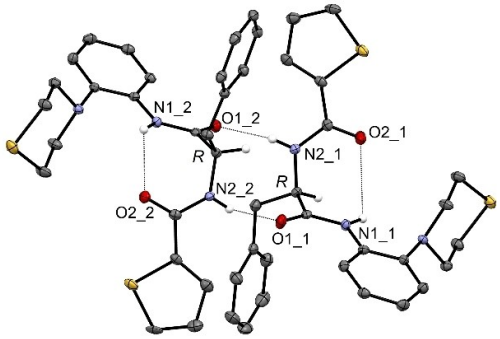

Figure 4. *Pseudo* centrosymmetric dimer in the crystal structure of the *R*-configured 2-thiomorpholinoanilide **25** (Figure 3; CSD refcode: JIHKOE).[38] Displacement ellipsoids are drawn at the 50% probability level. Positional disorder of the thiophene ring and carbon-bound H atoms except at the chirality center are omitted for clarity. Dashed lines represent hydrogen bonds. Color scheme: C, grey; H, white; N, blue; O, red, S, yellow.

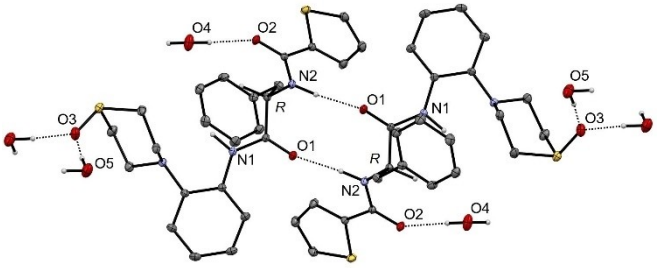

Figure 5. C_2-symmetric dimer in the crystal structure of the sesquihydrate of the 2-thiomorpholinoanilide sulfoxide **27** (Figure 3; CSD refcode: JIHLAR).[38] Displacement ellipsoids are drawn at the 50% probability level. Carbon-bound H atoms except at the chirality center are omitted for clarity. Dashed lines represent hydrogen bonds. Color scheme: C, grey; H, white; N, blue; O, red, S, yellow.

encountered in the solid-state structure of **25**. The $R_2^2(10)$ intermolecular N–H···O hydrogen bond motif is formed about a *pseudo* center of symmetry. The crystal structure of the corresponding sulfone **26** (CSD refcode: JIHKUK) and that of its *N*α-2-fluorobenzoyl derivative **28** (CSD refcode: KODROO),[39] one of the most potent compounds thus far (Section 4), are isomorphous to that of **25**.[38]

The $R_2^2(10)$ intermolecular N–H···O hydrogen bond pattern formed between the phenylalanine moieties of adjacent molecules is also conserved in the crystal structure of the sesquihydrate of the corresponding sulfoxide **27** (monoclinic system, space group *I*2, Z = 4).[38] In contrast to **25** and **26**, the hydrogen bond dimer in **27**·1.5 H_2O does not contain a *pseudo* inversion center but a crystallographic twofold rotation axis (Figure 5). The molecular conformation in the crystal structure of **27**·1.5 H_2O is somewhat different from those encountered in *rac*-**1**, **25**, **26** and **28**. The intramolecular N–H···O hydrogen bond is not observed in **27**·1.5 H_2O. Instead, the thiophenoyl oxygen atom (O2) accepts an O–H···O hydrogen bond from a water molecule. In contrast, the anilide nitrogen atom (N1) remains without a hydrogen bond acceptor in the crystal, which may be considered as an exception to Etter's first hydrogen bond rule for organic compounds, stating that all good proton donors and acceptors are used in hydrogen bonding.[51] As shown in Figure 5, the sulfoxide oxygen atoms (O3) each accept two O–H···O hydrogen bonds from solvent water molecules, demonstrating the hydrogen bond acceptor capabilities of these groups.

3. Biology

3.1. Screening Campaigns and Initial Hit Characterizations

In 2013, Ballell *et al.* reported a number of potent, non-cytotoxic small molecule hits for possible lead optimization against tuberculosis.[26] *Mycobacterium bovis* BCG, whose genome is > 99% identical to that of *M. tuberculosis* H37Rv,[52] was used as surrogate bacterium in the early phenotypic screening for reasons of biosafety. After the initial high-throughput screening of GSK's corporate compound collection ($> 2 \cdot 10^6$ compounds) against *M. bovis* BCG, the initial hit list was narrowed by applying similarity and physicochemical property filters, resulting in 3509 compounds that were progressed to dose-response studies of *M. bovis* BCG growth inhibition and HepG2 cytotoxicity. Applying the criteria of a therapeutic index IC_{50}(HepG2)/IC_{50}(*M. bovis* BCG) > 50 and a minimal inhibitory concentration (MIC) < 10 μM against *M. bovis* BCG yielded 777 compounds for which the MICs against *M. tuberculosis* H37Rv using Middlebrook 7H9 growth medium were determined. This resulted in a list of 177 compounds with MIC_{90} < 10 μM,[53] including compound **1** (GSK1055950A). For the latter, MIC_{90} = 7.6 μM against *M. tuberculosis* H37Rv was determined, but the hit was not selected for further characterization at that stage.[26] We note that in the supporting information of this work, the absolute configuration of GSK1055950 A is unspecified, whereas GSK17229177 was in included in the hit list as being the *S*-

enantiomer of **1** (Section 3.3). In a later work, GSK17229177 (*i.e. S*-**1**) was reported as inhibiting more than 50% of enzymatic activity of the *M. tuberculosis* cytidine triphosphate (CTP) synthetase PyrG.[54]

Three research groups reported on whole cell screenings of the Pathogen Box® library against NTM species at nearly the same time.[27] This library contained 400 drug-like compounds with cytotoxicity levels considered acceptable for early drug discovery. 129 of these compounds are known to be active against *M. tuberculosis* (including 13 reference compounds). Screening of known anti-TB actives against *M. abscessus* has been proposed as a strategy to accelerate drug discovery against this NTM species, as these compounds are expected to permeate the mycobacterial cell wall and likely have a homologous target in *M. abscessus*.[55] Low *et al.* performed a primary screening against *M. abscessus* Bamboo and *M. avium* 11, resulting in 13 *M. abscessus* hits and 33 *M. avium* hits.[27a] Compound *R*-**1** was among six double hits remaining after exclusion of reference compounds. The hits were confirmed by MIC_{90} determinations against *M. tuberculosis* H37Rv (1.7 μM), *M. abscessus* Bamboo (7 μM) and *M. avium* 11 (3 μM) using 7H9 medium. We performed a screening of the Pathogen Box® library and GSK's TB compound set[26] (568 compounds in total) against the reference strain *M. abscessus* ATCC19977 transformed to express the tomato red fluorescent protein (RFP), using a fluorescence readout, and identified 17 hits including compound *R*-**1**.[27b] Jeong *et al.* discovered activity of *R*-**1** against *M. abscessus* in a screening of the Pathogen Box® using a resazurin-based assay.[27c]

Using a target-based approach, Ebright and co-workers identified AAPs in a high-throughput screening of a library of ~114,000 synthetic compounds using a fluorescence-detected *in vitro* assay of promotor-dependent transcription by the *M. tuberculosis* RNAP σ^A holoenzyme.[28][56] Further assaying of 167 initial screening hits and exclusion of known RNAP inhibitors and DNA-binding compounds finally resulted in 15 compounds, including **DL-AAP1**, that showed whole cell activity against *M. tuberculosis* H37Rv *in vitro* with $MIC \leq 50\ \mu g\,mL^{-1}$.[28b] In order to evaluate the impact of the stereochemical configuration on the activity, the enantiomers **D-AAP1** and **L-AAP1** were separated and subjected to RNAP inhibition and *in vitro* growth inhibition assays. The results suggest that the inhibitory effect is stereospecific with the *R*-configured **D-AAP1** being the active enantiomer, while the *S*-configured **L-AAP1** is inactive (Table 1). For **D-AAP1** and **D-IX336**, it was also shown in this study that these compounds poorly inhibit the RNAPs of *Staphylococcus aureus* and *Escherichia coli*.

Table 1. Comparison of **AAP1** stereoisomers: *M. tuberculosis* RNAP σ^A inhibition and *in vitro* activity against *M. tuberculosis* H37Rv.[28a]

Compound[a]	*M. tuberculosis* RNAP σ^A IC_{50} (μM)	*M. tuberculosis* H37Rv MIC ($\mu g\,mL^{-1}$)[b]
DL-AAP1 (*rac*)	0.8	6.25
D-AAP1 (*R*)	0.4	3.13
L-AAP1 (*S*)	>50	>50

[a] The absolute configuration is given in parentheses. [b] Determined by microplate Alamar Blue assays.

3.2. Structural Basis of RNAP Inhibition

The identification of AAPs in a target-based screening and subsequent hit characterization (previous section) provided first evidence that the compound class exerts antimycobacterial activity through inhibition of the mycobacterial RNAP.[28a] In contrast to eukaryotes, bacteria express only one type of RNAP. The bacterial RNAP apoenzyme consists of five subunits, *viz.* two α (RpoA) subunits and each one β (RpoB), β′ (RpoC) and ω (RpoZ) subunit (Figure 6).[16] The $\alpha_2\beta\beta'\omega$ core enzyme adopts a claw-like structure with the β and β′ subunits resembling "pincers". The cleft between β and β′ features the main primary channel (1), the nucleoside triphosphate (NTP) entry channel (2) and the RNA exit channel (3). The Mg^{2+}-containing catalytic center of RNA synthesis is located at the base of the cleft. The bridge helix connects the β and β′ subunits. The trigger loop is a mobile structural component of the active site, which cycles between an open state to enable a NTP substrate to enter the site and closed state that holds the substrate at the site.[57]

Protein crystallographic studies have revealed insight into the structure of the mycobacterial RNAP and the binding modes of inhibitors. In 2017, Hubin *et al.* reported a crystal structure of the *Mycobacterium smegmatis* RNAP (2.76 Å resolution, PDB code: 5TW1).[58] Shortly thereafter, Lin *et al.* published a series of crystal structures of the *M. tuberculosis* RNAP alone and in complex with rifampicin and/or AAPs with resolutions around 4 Å, thereby establishing the structural basis of inhibition of the mycobacterial RNAP and thus revealing how transcription by these compounds is blocked.[28a] The results confirmed that rifampicin binds to the β subunit and sterically blocks the extension of RNA products of 2–3 nucleotides to afford longer RNA strands, as had been proposed previously.[59] The crystal structure determination of the *M. tuberculosis* open promoter complex (RPo) co-crystallized with **D-AAP1** was achieved by soaking of pre-formed crystals of the *M. tuberculosis* RPo with the respective compound.[28a] The RPo represents a conforma-

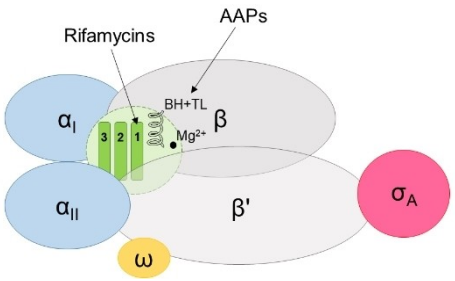

Figure 6. Schematic representation of the mycobacterial RNAP σ^A holoenzyme, illustrating the binding sites of rifamycins and AAPs. Two α subunits (blue), the β and β′ subunits (grey) and the ω subunit (yellow) constitute the core enzyme. The factor σ^A (red) is required to initiate transcription. The channels 1, 2 and 3 and the Mg^{2+}-containing catalytic site are located in the cleft between β and β′. Abbreviations: BH, bridge helix; TL, trigger loop. The figure was adapted with permission.[16a] Copyright 2022, The Royal Society of Chemistry.

tion of the RNAP holoenzyme with bound promoter DNA.[16b] Replacement of **D-AAP1** by **D-IX336** (Scheme 2) followed by X-ray diffraction and selenium anomalous dispersion analysis confirmed the identified binding site, orientations and inhibitor interactions (PDB code: 5UHF).[28a] As shown in Figures 7A and B, AAPs bind to the β and β′ subunits at a site located at the N terminus of the above-mentioned bridge helix. Three pocket-like subsites accommodate the three AAP aryl rings. A crystal structure of the *M. tuberculosis* RPo in complex with both **D-AAP1** and rifampicin provided clear evidence that the binding sites are different and not overlapping (Figure 7C), as shown schematically in Figure 6, and that both inhibitors can bind simultaneously to the mycobacterial RNAP.[28a]

Figure 7D gives a summary of inhibitor interactions of **D-AAP1** with the *M. tuberculosis* RPo. Substitution of alanine for the arginine residue βR562A (βR637A) resulted in resistance to AAPs, which was evident from both RNAP-inhibitory activity and whole cell activity, providing further confirmation of the identified AAP binding site and the importance of the encountered intermolecular interactions.[28a] The non-overlapping binding sites of AAPs and rifampicin in the crystal structure suggested that the compound classes should not exhibit cross-resistance, which was confirmed experimentally. Substitution in the AAP binding site led to resistance to **D-AAP1** but not to rifampicin and *vice versa*, as demonstrated by whole cell activity measurements.[28a] The cellular target was also identified in *M. tuberculosis* and in the fast-growing NTM species *M. smegmatis* by genetic analysis of resistant mutants.[28b]

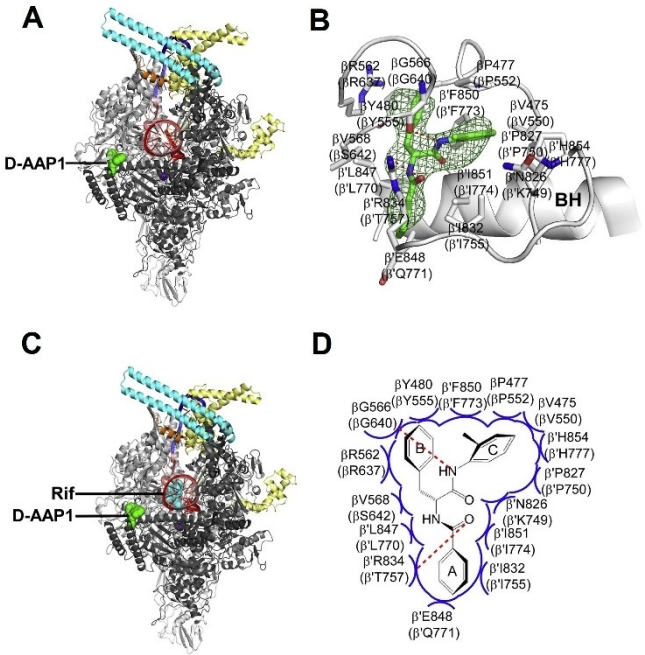

Figure 7. (A) Overall structure and (B) inhibitor interactions of the *M. tuberculosis* RPo in complex with **D-AAP1** (PDB code: 5UHE). The green mesh shows the mF_o-F_c electron density omit map for **D-AAP1** (contoured at 2.5σ). Residue numbers in parentheses are as in the *Escherichia coli* RNAP. (C) Overall structure of the *M. tuberculosis* RPo in complex with both **D-AAP1** and rifampicin (PDB code: 5UHG). (D) Summary of **D-AAP1** interactions (red dashed lines represent hydrogen bonds; blue arcs show van der Waals interactions). Abbreviations: Rif, rifampicin; BH, bridge helix. The DNA template strand is colored in red in panels A and C. The figure was adapted with permission.[28a] Copyright 2017, Elsevier.

Based on the target validation of AAPs in *M. tuberculosis*, Low *et al.* hypothesized that compound *R*-**1**, which they had identified as a hit in a phenotypic screenings against *M. abscessus* and *M. avium* (Section 3.1), possibly also inhibits the RNAP in these NTM species.[27a] In order to confirm the target in *M. abscessus* experimentally, Mann *et al.* isolated and characterized six strains of *M. abscessus* Bamboo exhibiting spontaneous resistance to *R*-**1** ($MIC_{90} > 100$ μM).[60] The mutations found in these six strains affected amino acid residues near the binding site, which was inferred from a homology model based on the *M. tuberculosis* RNAP. This lends support to the view that AAPs also exert activity against this NTM species through inhibition of the RNAP.

It is worth mentioning that the binding site of AAPs is similar to that of CBR compounds, which inhibit the RNAP of Gram-negative bacteria but not the mycobacterial RNAP.[16a] Structural differences in these enzymes should account for the observed selectivity. Although both compound classes bind to the bridge helix, the *E. coli* RNAP has a two-pocket binding site complementary to the two aryl rings of CBR compounds, in contrast to the three-pocket site in the *M. tuberculosis* RNAP, complementary to the three aryl rings of AAPs.[28a] In this context it is interesting to note that Mazumder *et al.* showed that CBR703 and the AAP **IX214a**[30] (among other compounds) inhibit trigger loop closure of the *E. coli* RNAP active site in solution.[57]

3.3. Antimycobacterial Evaluation

The prototypical compound **D-AAP1** (*R*-configured) was identified as a selective and stereospecific inhibitor of the *M. tuberculosis* RNAP (Section 3.1).[28] The observed stereospecific inhibition of the enzyme coincides with stereospecific activity against *M. tuberculosis* H37Rv *in vitro* (Table 1). We are not aware of an RNAP inhibition assay for both enantiomers of the whole cell screening hit **1**.[61] We, however, investigated *in vitro* growth inhibition of *M. smegmatis* and *M. abscessus* for both *R*-**1** and *S*-**1**.[34] The results are consistent with those observed for **D-AAP1** and **L-AAP1** and *in vitro* activity against *M. tuberculosis* (Table 1),[28a] which show that *R*-**1** is active against *M. smegmatis* ($MIC_{90} = 0.78$ μM) and *M. abscessus* ($MIC_{90} = 6.25$ μM) *in vitro* whereas *S*-**1** is not ($MIC_{90} > 100$ μM).[34] *R*-**1** was also found to be active against *M. tuberculosis* with reported MIC_{90} values around 1 μM.[27a,38] By way of comparison, for rifampicin, $MIC_{90} = 0.06$ mg L^{-1} (0.07 μM) against *M. tuberculosis* H37Rv in 7H9 medium supplemented with 10% albumin-dextrose-saline and 0.05% polysorbate 80 can be found in the literature.[62]

As mentioned in section 3.1, the hit list resulting from the GSK screening campaign against *M. tuberculosis* notably contains **1** (GSK1055950A) with unspecified absolute configuration ($MIC_{90} = 7.6$ μM) and, interestingly, *S*-**1** (GSK17229177) with $MIC_{90} = 6.6$ μM.[26] This suggests that further investigation may be warranted in light of the aforementioned stereospecific activity observed for **D-AAP1** *versus* **L-AAP1**[28a] and *R*-**1** *versus* *S*-**1**.[34]

Consistent with the observed selective inhibition of the isolated mycobacterial RNAP by **D-AAP1** and **D-IX336**, Lin *et al.* found that the two compounds inhibit growth of *M. tuberculosis*, *M. smegmatis* and *M. avium in vitro* but are not active against *S. aureus* and *E. coli*, which are examples representative of Gram-positive and Gram-negative bacteria, respectively (Table 2).[28a] Interestingly, **DL-AAP1** was found to be inactive (MIC $>50\ \mu g\,ml^{-1}$) against the fast-growing NTM species *Mycobacterium phlei*, *Mycobacterium hassacium* and *Mycobacterium thermoresistibile*,[28b] the latter of which is known to cause disease in humans.[63] It was hypothesized that the inactivity of the compound against these NTM species can be attributed to poor cellular uptake or efflux pumps.[28b]

As mentioned above, the screening hit *R*-**1** was found active against *M. tuberculosis*, *M. smegmatis*, *M. avium* and *M. abscessus*.[27,34] We performed further *in vitro* antimycobacterial evaluation of the compound and a variety of derivatives.[38] For the reference strain *M. abscessus* ATCC19977, we also investigated dependency of MICs on the growth medium. The results for *R*-**1**, the thiomorpholine analogue **25**, its sulfone **26** and sulfoxide **27** are summarized in Table 3. The compounds exhibit potent *in vitro* activity against these clinically relevant mycobacterial strains, including the NTM species *Mycobacterium intracellulare*, which belongs to the MAC (Section 1), and the clinical isolate *M. abscessus* Bamboo.[64] For the *M. abscessus* reference strain, the MIC_{90} values determined using Mueller-Hinton II (MHII) broth (cation-adjusted) tend to be somewhat higher than those determined using Middlebrook 7H9 medium. The compounds, however, except for **25** retain antimycobacterial activity in both media, which is a desirable trait of antibacterial agents. Loss of activity in MHII medium was also observed for other thiomorpholine analogs of *R*-**1**.[38]

Table 2. MICs ($\mu g\,ml^{-1}$) of **D-AAP1** and **D-IX336** against *M. tuberculosis*, *M. smegmatis*, *M. avium* and representative Gram-positive and Gram-negative bacteria.[28a]

	D-AAP1	D-IX336[b]
M. tuberculosis H37Rv[a]	3.13	6.25
M. smegmatis mc^2 155[b]	0.78	0.78
M. avium ATCC 25291[a]	6.25	12.5
S. aureus ATCC12600	>25	>25
E. coli D21f2tolC (*rfa tolC*)	>25	>25

[a] Determined by microplate Alamar Blue assays. [b] Middlebrook 7H9 medium supplemented with 0.5% glycerol and 0.05% polysorbate 80.

Table 3. MIC_{90} values (μM) of *R*-**1**, **25**, **26** and **27** against several mycobacterial strains, based on optical density measurements. Experimental details of the assays can be found in the literature.[38]

	Medium	*R*-1	25	26	27
M. tuberculosis H37Rv	7H9[a]	0.78	6.25	0.2	0.4
M. smegmatis mc^2 155	7H9[a]	0.78	3.13	1.56	1.56
M. abscessus ATCC19977	7H9[a]	6.25	6.25	1.56	3.13
M. abscessus ATCC19977	MHII[b]	12.5	>100	3.13	6.25
M. abscessus Bamboo	7H9[a]	4.4	14	1.7	2
M. intracellulare ATCC35761	7H9[a]	0.39	0.39	0.1	0.1

[a] Middlebrook 7H9 medium supplemented with 10% albumin-dextrose-saline and 0.05% polysorbate 80. [b] Mueller-Hinton II broth (cation-adjusted) supplemented with 0.05% polysorbate 80.

Mann *et al.* conducted an in-depth *in vitro* profiling study of the hit compound *R*-**1** against *Mycobacterium abscessus*, including susceptibility testing against the subspecies *M. abscessus* subsp. *bolletii* and *M. abscessus* subsp. *massiliense* as well as clinical isolates.[60] The latter two subspecies are known to exhibit antibiotic susceptibilities different from that of the reference strain *M. abscessus* subsp. *abscessus* (ATCC19977).[65] It was shown that MIC_{90} values determined in 7H9 medium by optical density measurements are essentially comparable (5.4–10 μM) for the three *M. abscessus* subspecies and the ten clinical isolates studied.[60] For the sake of comparison, MIC_{90} values around 10 μM against *M. abscessus* ATCC19977 in Middlebrook 7H9 broth were reported for rifampicin, while those reported for rifabutin are lower by about an order of magnitude.[60,66]

In vitro bactericidal activity of *R*-**1** and derivatives against *M. abscessus* ATCC19977 has also been studied,[38,60] as this property is crucial for effective antimycobacterial therapy, especially for the treatment of *M. abscessus* infections.[67] The minimum bactericidal concentration (MBC) of an antibiotic agent actively reduces the number of colony forming units in an inoculum by more than a chosen threshold, *e.g.* 99.0% (MBC_{99}), after a defined incubation time. The MBC/MIC ratio is usually ≤ 4 for bactericidal and >4 for bacteriostatic agents.[68] For *R*-**1**, $MBC_{99} = 50\ \mu M$ was determined after four days of incubation, which is eight times larger than the MIC_{90} (6.25 μM). Compound **23**, however, exhibits a MBC_{99} of 6.25 μM, which is about four times larger than the optical density-based MIC_{90} in 7H9 medium (1.56 μM).[38]

Activity against intracellular mycobacteria is particularly desirable for new antimycobacterial agents, because of the mycobacterial pathogens' ability to survive and replicate in various cell types of a human host.[8b,69] For *M. abscessus*, for example, it has been demonstrated that antibiotic susceptibility in biofilms and macrophages differs from that of planktonic bacteria.[70] Intracellular activity for a compound is also an important factor to quantify *in vivo* activity in mouse models of TB.[26] Sorrentino *et al.* developed intracellular screening for compounds that inhibit growth of *M. tuberculosis* in human macrophages.[71] By a luciferase assay using luminescence, they determined an intracellular MIC_{90} of 1.85 μM against *M. tuberculosis* H37Rv in human monocytic THP-1 cells for compound **1** (GSK1055950 A),[71] which is about four times lower than the previously reported extracellular MIC_{90} against *M. tuberculosis* (7.6 μM).[26] Richter *et al.* reported a fluorescence-based assay for a THP-1 infection model for screening of compounds against intracellular RFP-expressing *M. abscessus* ATCC19977 and were the first to demonstrate intracellular activity of *R*-**1** against *M. abscessus* ($MIC_{90} = 36.2\ \mu M$).[72] In contrast, rifampicin proved inactive against *M. abscessus* ATCC19977 inside THP-1 cells, whereas an intracellular MIC_{90} of 5.5 μM was determined for

rifabutin under these conditions.[60] Mann *et al.* also investigated bactericidal activity of *R*-**1** against intracellular *M. abscessus* in the THP-1 infection model and determined an MBC_{90} of 16 μM after four days of incubation, which is virtually equal to the intracellular MIC_{90} they reported.[60]

Since pharmacotherapy of tuberculosis and NTM infections usually requires multidrug regimens, susceptibility testing of drug combinations *in vitro* is occasionally performed at early stages of antimycobacterial drug discovery. The ability of AAPs and rifampicin to bind to the *M. tuberculosis* RNAP simultaneously with non-overlapping binding sites (Figure 7C) suggested that combinations of compounds of both classes could be favorable. In order to verify this prediction experimentally *in vitro*, checkerboard interaction assays were carried out. Lin *et al.* tested the combination of **D-AAP1** and rifampicin against *M. smegmatis* mc^2 155.[28a] Based on fractional inhibitory concentration index (FICI) calculations, they concluded that the inhibitor-inhibitor interaction of this combination was additive. Mann *et al.* conducted *in vitro* susceptibility testing of *R*-**1** in combination with a variety of approved antibiotics of different classes against *M. abscessus* in broth and in the THP-1 infection model.[60] For the majority of the antibiotics, FICI calculations revealed an additive effect for the combination with *R*-**1**. The combination of *R*-**1** with the macrolide clarithromycin showed synergistic effects in broth and intracellularly. The authors reasoned that *R*-**1** might suppress inducible macrolide resistance conferred by the *erm*(41) gene in the *M. abscessus* reference strain,[73] as previously shown for the RNAP inhibitor rifabutin of the rifamycin class.[74]

4. Hit-To-Lead Optimization and SAR

The promising *in vitro* activity of the AAP screening hits against clinically relevant mycobacterial strains, including *M. tuberculosis*, *M. avium* and *M. abscessus*, and their modular structure rendered **D-AAP1** and *R*-**1** attractive as starting points for hit-to-lead optimization. In contrast to target-based approaches, phenotypic screenings, in which hit compounds are identified by their *in vitro* antimycobacterial activity, circumvent a discrepancy between target-based activity data and MICs.[26] In particular in antimycobacterial drug discovery, permeability issues likely account for such a discrepancy because of the waxy nature of the mycobacterial cell wall.[75] For advancing whole cell-based screening hits, it is, however, important to identify the cellular target. As described in detail above, the mycobacterial RNAP has been identified and validated as the target of AAPs by a target-based high-throughput screening[28a] independent of whole cell screenings,[26–27] structural biology efforts[28a] and genetic approaches.[28b,60] Protein crystallographic studies of the *M. tuberculosis* RNAP in complex with **D-AAP1** and **D-IX336** (Section 3.2) and *in silico* work on binding of *R*-**1** to a homology model of the *M. abscessus* RNAP[60] provided the structural basis for structural optimization of AAPs. Hit-to-lead optimization solely driven by whole cell antimycobacterial activity can be challenging in terms of rationalizing structure-activity-relationships (SAR), because alteration of compound permeability can also modulate antimycobacterial activities in addition to changes in target binding properties.[26]

In a 2015 patent, Ebright and colleagues disclosed more than 200 in the vast majority racemic AAP derivatives and their whole cell activity data (MICs) against *M. smegmatis*, *M. tuberculosis* and in part *M. avium*.[30] *M. tuberculosis* RNAP inhibitory activities (IC_{50}) for selected compounds were also included. Recently, we reported a set of about 25 enantiopure *R*-configured AAPs derived from the screening hit *R*-**1** and their activity data against *M. tuberculosis* and some NTM species, including *M. abscessus* (Table 3).[38] From these studies, SAR for AAPs could be deduced, which we summarize in the following paragraphs.

Figure 8 illustrates the sites in hit compound *R*-**1** that can be readily modified (*cf.* Scheme 5). As described in section 3.3, we found that change of the *R* configuration at the α-carbon atom (highlighted in green) to *S* results in virtually complete loss of antimycobacterial activity,[34] which is consistent with the results observed for *R*-configured **D-AAP1** *versus* *S*-configured **L-AAP1**.[28] Thus, the lead optimization studies have focused on *R*-configured or racemic derivatives. The impact of substitution at the α-carbon atom on the antimycobacterial activity has not yet been unveiled, as far as we are able to ascertain. *N*α-Methyl *R*-**1** showed no antimycobacterial activity,[39] which seems to confirm the importance of an N–H···O hydrogen bond to the protein backbone for binding to the RNAP, as indicated by *in silico* work (Figure 9A).[38]

The phenylalanine amide side chain (highlighted in yellow) has also been subjected to structural modification. The study by Ebright and colleagues revealed that the MICs are particularly sensitive to alterations of this part. Indeed, the phenyl group was retained in the most potent compounds. Introduction of a *p*-hydroxyphenyl group (*i.e.* replacement of the phenylalanine building block by tyrosine) and its acetyl and benzoyl derivatives decreased antimycobacterial activities, which was also observed for the corresponding *m*-hydroxyphenyl group.[30] The activity loss for tyrosine analogues was pronounced in the *M. abscessus* THP-1 infection model, which was attributed to increased polarity and, thus, decreased permeability of the compounds.[38] Interestingly, an opposite trend was observed against *M. intracellulare* in broth, where presence of the *p*-hydroxy group increased activity. *In silico* work indicated that

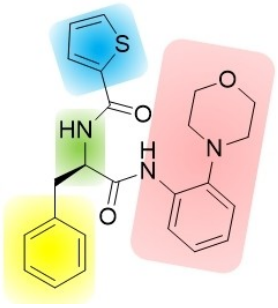

Figure 8. Chemical diagram of the screening hit *R*-**1**, highlighting groups attractive for structural alterations for SAR studies and lead optimization.

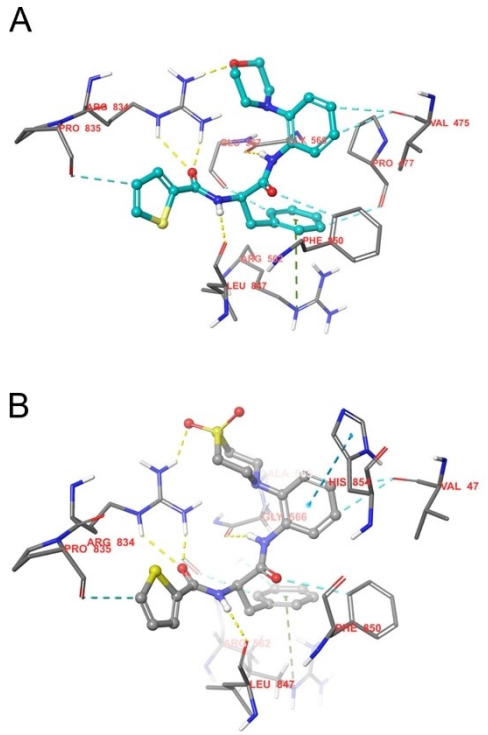

Figure 9. Docking poses of *R*-**1** (A) and **26** (B) and the β and β′ subunits of the *M. tuberculosis* RNAP (based on PDB entry 5UHE; *cf.* Figure 7). Color scheme: C, turquoise for the ligand in A, otherwise grey; H, white; N, blue; O, red, S, yellow. Dashed yellow lines illustrate hydrogen bonds. The figure was adapted with permission.[38] Copyright 2023, American Chemical Society.

the *p*-hydroxy group possibly forms a hydrogen bond to the RNAP protein backbone.[38]

As for the *N*α-aroyl moiety (highlighted in blue), reviewing the work by Ebright and colleagues revealed that a 2-thiophenoyl group, as in the screening hit *R*-**1**, or a 2-fluorobenzoyl moiety appears to be beneficial to antimycobacterial activity.[30] Therefore, we decided to center our attention to these two groups in our SAR study.[38] We should note, however, that also *N*α-2-methylbenzoyl derivatives were among the compounds that reached submicromolar MICs against *M. tuberculosis* and *M. avium*.[30,39] In general, we found similar MIC_{90} values against several mycobacterial strains in broth for the test compounds bearing either an *N*α-2-thiophenoyl or an *N*α-2-fluorobenzoyl group. The latter proved beneficial to intracellular activity in the *M. abscessus* THP-1 infection model, which could be due to higher permeability of the *N*α-2-fluorobenzoyl derivatives.[38] Recently, we expanded our SAR study to include some 2,6-disubstituted *N*α-benzoyl groups to sterically shield the amide bond with the aim of increasing microsomal stability (Section 5.2). We found that 2,6-difluorobenzoyl and 2-fluoro-6-methylbenzoyl moieties are well tolerated, whereas the sterically more demanding 2,6-dimethylbenzoyl group causes a decline in antimycobacterial activity.[39]

Evaluation of the crystal structure of **D-AAP1** in complex with the *M. tuberculosis* RNAP (Section 3.2) revealed that the 2-methyl group on the AAP *N*-aryl ring of the ligand (ring C in Figure 7D) points towards a void that could be sufficiently large to accommodate at least six additional non-hydrogen atoms.[28a] Interestingly, the 2-morpholinoanilide group in the hit compound *R*-**1** (highlighted in red in Figure 8) exhibits five additional non-hydrogen atoms compared with the *N*-*o*-tolyl group in **D-AAP1**. Molecular docking of *R*-**1** to the β and β′ subunits of the *M. tuberculosis* RNAP indicated that the morpholino oxygen atom appears to serve as hydrogen bond acceptor for the side chain of an arginine residue of the backbone (Figure 9A).[38] Replacement of morpholine by thiomorpholine in **25** (Figure 3) results in loss of antimycobacterial activity (Table 3), which appears to be consistent with a weaker hydrogen bond acceptor strength of the thiomorpholine sulfur atom. The corresponding sulfone **26** and sulfoxide **27** (Figure 3) exhibited antimycobacterial activities comparable with or higher than *R*-**1**.[38] According to the docking studies, thiomorpholine sulfone in **26** (Figure 9B) and sulfoxide in **27** act as hydrogen bond acceptor for the arginine side chain similar to morpholine in *R*-**1**. It is, however, interesting to note that Ebright and colleagues also found submicromolar activities for compounds bearing a methoxy or fluoromethoxy group in 2-position on the AAP *N*-aryl ring, *e.g.* in **IX276** (Figure 10).[30] This indicates that six additional non-hydrogen atoms on this site and hydrogen bonding to the arginine residue may not be crucial for potent antimycobacterial activity. Like *N*α-methylation (*vide supra*), introduction of a methyl group at the anilide nitrogen atom in *R*-**1** resulted in complete loss of antimycobacterial activity.[39] Similarly, the inability of the *N*-methyl anilide to form an N–H···O hydrogen bond in the binding pocket, as revealed by the docking pose (Figure 9A),[38] most likely accounts for the observed loss of activity.

To shed light on the role of the tertiary nitrogen atom of the (thio)morpholine ring, we also synthesized the corresponding tetrahydrothiopyran derivatives of **22** and **23** (Section 2.2). Replacement of the tertiary nitrogen atom by a CH group proved to be detrimental to *in vitro* activity.[38] The docking poses suggest that the tertiary (thio)morpholine nitrogen atom possibly also approaches the arginine side chain in the binding site as a hydrogen bond acceptor (Figure 9).

We also investigated the impact of a fluorine substituent on the AAP *N*-aryl ring in *meta* and *ortho* position to the amide group.[38–39] We hypothesized that a fluorine substituent in these positions could impede hydrolysis of the anilide bond through

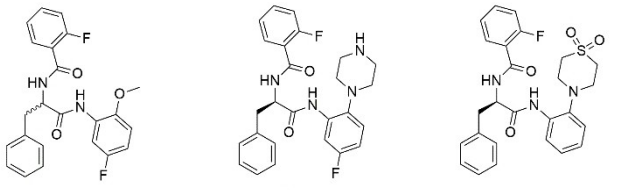

M. tuberculosis: 0.39 μM
M. avium: 1.9 μM

M. tuberculosis: 1.62 μM
M. avium: 0.42 μM

M. tuberculosis: 0.2 μM
M. abscessus: 0.78 μM

Figure 10. Chemical diagrams and MIC_{90} values against *M. tuberculosis* H37Rv, *M. avium* ATCC25291 or *M. abscessus* ATCC19977 of three of the most potent AAPs disclosed by Ebright and colleagues (**IX276** and **IX214a**)[30] and Lang *et al.* (**28**).[38] For easier comparison, MICs for **IX276** and **IX214a** were converted from μg mL^{-1} to μM.

steric effects or might prevent metabolic hydroxylation of the aromatic ring. In general, however, introduction of a fluorine substituent in *meta* position decreased activities against the mycobacterial strains tested in broth but increased those against intracellular *M. abscessus*.[38] A fluorine atom in *ortho* position increased MIC_{90} values roughly by an order of magnitude, whereas introduction of an *ortho* methyl group resulted in complete loss of antimycobacterial activity.[39]

Figure 10 depicts chemical diagrams and selected *in vitro* activity data for two of the most potent compounds disclosed by by Ebright and colleagues[30] and one of the most advanced compounds, we obtained by lead optimization driven by whole cell activity against the NTM species *M. abscessus*.[38–39] Figure 11 summarizes the SAR results from the latter study. In brief, a D-phenylalanine building block, an *N*α-2-fluorobenzoyl or an *N*α-2-methylbenzoyl group and an aniline building block bearing a six-membered saturated ring with hydrogen bond acceptor capability seem to be favorable for antimycobacterial activity *in vitro*.

5. Physicochemical and Pharmacokinetic Properties

5.1. Physicochemical Properties

In general, the AAPs studied exhibit molecular weights (< 500 Da)[30] and hydrophobicity ($logP < 5$)[38] in the range favorable for drug-like molecules to exhibit oral bioavailability.[76] Solubility is another important physicochemical property in drug discovery.[77] We determined kinetic (or apparent) solubilities for a set of AAPs in the course of our lead optimization study.[38] It can be helpful to undertake kinetic solubility measurements at early stage of drug discovery in order to avoid limiting or compromising the outcomes by solubility issues during later *in vitro* and *in vivo* experiments.

Table 4 lists some physicochemical properties for *R*-**1** and **25**–**28**. As expected,[78] the thiomorpholine derivative **25** is more hydrophobic and less soluble in phosphate-buffered saline than *R*-**1** with a morpholine ring. The thiomorpholine sulfone congener **26** is still more hydrophilic and more soluble than **25**. Remarkably, the kinetic solubility of the thiomorpholine sulfoxide **27** is higher than that of **26** by an order of magnitude. We observed a similar trend for other AAPs with a thiomorpholine sulfoxide group attached to the *N*-aryl ring.[38] Higher polarity and thus higher aqueous solubility of sulfoxides compared to the corresponding sulfones is well known. This property could also open up the possibility of administering drugs as sulfoxide prodrugs, which are metabolically converted to the corresponding sulfone.[78] In favorable cases, this approach could afford higher plasma and tissue levels of active compounds than direct administration of the sulfone drug. Here it is interesting to point out that the clogP values are not good predictors of aqueous solubility in the case of sulfone *versus* sulfoxide (Table 4).

The majority of the AAPs that we studied exhibited $clogP > 3.5$ and displayed kinetic solubilities $< 50\ \mu M$, which might be less than favorable for performance in biological assays. Against *M. abscessus*, compounds with clogP values within the range 2–3 achieved the lowest extracellular MICs. In the *M. abscessus* THP-1 infection model, a direct relationship between clogP values and intracellular MICs was not obvious. Nevertheless, the most active AAPs against intracellular *M. abscessus* exhibit clogP values around 2.8.[38] These *in vitro* data suggest that clogP values within 2.5–3 appear to be desirable for antimycobacterial AAPs. For lead-like molecules, $logP \leq 3$ has also been proposed as a molecular filter in fragment-based drug discovery.[79]

5.2. Pharmacokinetic Properties

The *in vitro* pharmacokinetic (PK) properties for compounds contained in the Pathogen Box® library, and thus for *R*-**1**, were supplied by MMV.[80] Table 5 lists a selection of these data for *R*-**1**. Inhibition of CYP enzymes with estimated IC_{50} values in the micromolar range is less favorable for drug candidates. According to the listed effective permeability (PAMPA assay),[80]

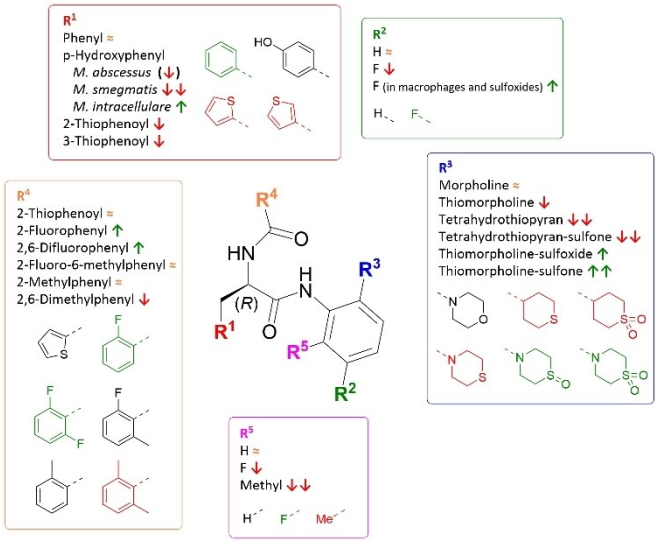

Figure 11. Summary of SAR results for *in vitro* antimycobacterial activity of AAPs by Lang *et al.*[38–39] Green arrows indicate an increase and red arrows a decrease of activity with respect to *R*-**1**. The figure was adapted with permission.[38]

Table 4. Molecular weights (MW), clogP values and kinetic solubilities of AAPs *R*-**1** and **25**–**28**.[38]

	MW (Da)	clogP[a]	Solubility (μM)[b]
R-**1**	435.54	3.72	82
25	451.60	4.45	34
26	483.60	2.54	62
27	467.60	2.49	271
28	495.57	2.71	64

[a] Calculated with ChemDraw. [b] Determined by nephelometry. Medium: phosphate-buffered saline (pH 7.4, 2% DMSO).

Table 5. Selected *in vitro* PK data for *R*-**1** from the Pathogen Box® library.[80]

CYP2D6[a] IC_{50} (μM)	CYP3 A4[a] IC_{50} (μM)	PAMPA[b] (10^{-6} cm s^{-1})	Mouse plasma stability (%)[c]	Fraction unbound (mouse) PPB[d]
2.05	1.39	14.4	60	0.024

[a] Fluorescence screening assay in human liver microsomes (estimated IC_{50}). [b] Parallel artificial membrane permeation assay (PAMPA). Effective permeability: pH 6.5; 1 μM substrate. [c] % remaining after 4 h incubation in mouse plasma at 37 °C; 1 μM substrate. [d] Plasma protein binding (PPB); mouse plasma equilibrium dialysis; 37 °C, 1 μM substrate.

R-**1** can be roughly classified as a moderately permeable compound with regard to oral absorption.[81]

Lang *et al.* subjected the hit compound *R*-**1** and **28** to *in vitro* plasma and stability testing in suspensions of liver microsomes, as a model for hepatic stability and as an indicator of intrinsic clearance of AAPs.[38] Both compounds proved stable in human plasma over the time studied (2 h). Compound **28** was also found to be stable in murine plasma over the same time. In contrast, only 60% of the initial concentration of *R*-**1** remained after two hours of incubation in mouse plasma. The latter observation appears to be consistent with the mouse plasma stability of *R*-**1** listed in the Pathogen Box® library *in vitro* PK dataset (Table 5).[80] *N*α-Methylation of *R*-**1** had no pronounced impact, whereas a methyl group at the anilide nitrogen atom in *R*-**1** increased the stability in murine plasma.[39] It was further shown that substituting thiomorpholine dioxide for morpholine and replacement of the *N*α-2-thiophenoyl group by 2-fluorobenzoyl or 2-methylbenzoyl increased the stability in mouse plasma.[38–39] The Pathogen Box® library dataset lists human and mouse liver microsomal half-lives of respectively 129 min and 795 min for *R*-**1**. In contrast, Lang *et al.* reported microsomal half-lives of the order of minutes for both *R*-**1** and **28**. Possibly the addition of NADPH to the assay medium (3 mM) in the study by Lang *et al.* made a difference.[38] The assay conditions have not been disclosed with the Pathogen Box® data. The intrinsic clearance in human liver microsomes of *R*-**1** in the Pathogen Box® library dataset (0.668 L h^{-1} kg^{-1}) is also lower than that reported by Lang *et al.* (81960 L h^{-1} kg^{-1}).[38] The *N*-methyl derivatives of *R*-**1** did not exhibit improved microsomal stability, whereas an *ortho* methyl group on the aniline moiety in **28** appeared to be beneficial.[39] Lang *et al.* hypothesized that the low microsomal stability of *R*-**1** accounts for the poor oral bioavailability in rodents.[38] The low fraction unbound in mouse plasma (Table 5) suggests that protein binding might be an important factor in this regard.[82]

Intravenous and oral PK data for *R*-**1** in male Sprague Dawley rats ($n = 2$) provided by MMV[80] (also listed in ref.[27a]) indicate that the oral bioavailability is very low ($F < 1\%$). After oral administration of a 5 mg kg^{-1} body weight dose, a maximum plasma concentration $c_{max} = 2.28$ ng mL^{-1} (0.005 μM) was observed at $t_{max} = 0.375$ h. Mann *et al.* conducted a study of *in vivo* PK properties of *R*-**1** in female CD-1 mice ($n = 2$).[60] They orally administered a single dose of 25 mg kg^{-1} body weight and reported a maximum plasma concentration of 0.07 μM. The plasma levels observed in these two preliminary PK studies in rodents are lower than the extra- and intracellular MIC levels of *R*-**1** against mycobacteria by at least an order of magnitude (*cf.* Table 3).

6. Cytotoxicity Assessment

Cytotoxicity is critical property in small-molecule drug discovery. Apart from the desired interaction with a particular target, drug candidates and their metabolites can interfere with the function of other biomolecules in humans and thereby cause cellular damage leading to cell stress or cell death.[83] Therefore, it is important to identify cytotoxic compounds early in drug discovery programs.

Lin *et al.* reported that **D-AAP1** did not inhibit the human RNAP I, RNAP II and RNAP III ($IC_{50} > 25$ μM) and showed poor activity against mammalian cells (Vero E6) up to 25 μg mL^{-1}.[28a] Likewise the majority of AAPs disclosed in a patent by Ebright and colleagues exhibited minimum cytotoxic concentrations > 25 μg mL^{-1} against Vero E6 cells.[30] As mentioned in Section 3.1, compounds cytotoxic against HepG2 (a human liver cancer cell line) were excluded in the screening of the GSK compound library, in which antimycobacterial activity of compound **1** was discovered.[26] For *R*-**1**, the Pathogen Box® dataset lists a cytotoxic concentration (CC_{20}) of 27.6 μM against HepG2 cells.[80]

As a single *in vitro* cell viability test is considered insufficient to assess cytotoxicity,[84] we tested *R*-**1** and derivatives against a variety of mammalian cell lines.[34,38–39] With a few exceptions that showed weak cytotoxic effects, the compounds, including the most potent ones, were found to be non-toxic against the cell lines tested with $EC_{50} > 30$ μM.[38] Notably *R*-**1** and **28** at 50 μM concentration, however, reduced the viability of HEK293 cells (a human kidney cell line) by 33% and 27%, respectively, after 24 hours compared to a DMSO-treated control, whereas the majority of the AAPs studied did not reduce the cell viability by more than 10%.[39] Interestingly, among the AAPs studied, *N*α-methyl *R*-**1** exhibited the most pronounced cytotoxicity against HEK293 cells under the aforementioned conditions.

7. Conclusions and Future Perspectives

Several screening campaigns identified AAPs as potent agents active against *M. tuberculosis* and clinically relevant NTM species. The β and β′ subunits of the mycobacterial RNAP were validated as the molecular target in *M. tuberculosis* H37Rv and *M. abscessus* ATCC19977 by structural biology efforts and/or genetic approaches. The new mechanism of action, *viz.* inhibition of the mycobacterial RNAP through binding to the enzyme at a site different from that of RNAP inhibitors of the rifamycin family, and bactericidal properties *in vitro* are promising characteristics of the AAP compound class. Their modular structure and the relative ease of their racemization-free synthesis make AAPs attractive for lead optimization programs,

which have led to candidates exhibiting submicromolar MICs against several clinically relevant mycobacteria. The *R* configuration of the chirality center at the α-carbon atom appears to be critical for target binding and antimycobacterial activity. Small molecule X-ray crystallography revealed that the crystal structures of AAPs are dominated by intra- and intermolecular N–H···O hydrogen bonding between amide groups. The phenylalanine amide core has been shown to be sensitive to substitution, whereas a *N*α-2-thiophenoyl or *N*α-2-fluorophenyl group is favorable for activity. The results of *in vitro* and pilot *in vivo* PK studies are, however, less favorable and have hampered progression of the compounds to *in vivo* pharmacodynamics studies thus far. Nonetheless, in view of the promising *in vitro* activity, especially against *M. abscessus*, and the urgent need for antimycobacterial drugs with a new mechanism of action, further investigation of this compound class seems to be justified. Gaining insight into the metabolic fate in plasma and liver microsomes will be important to inform future research on AAPs. Further chemical modification and formulation science will be needed to overcome the unfavorable PK properties in order to develop AAPs to be effective in *in vivo* models of TB and NTM infections.

Author Contributions

Rüdiger W. Seidel: Conceptualization, writing – original draft preparation and visualization. Richard Goddard: Conceptualization, writing – review and editing. Markus Lang: Visualization, writing – review and editing. Adrian Richter: Conceptualization, writing – review and editing, supervision and funding acquisition.

Acknowledgements

We would like to thank our present and former colleagues Lea Mann, Ilaria Sequenzia, Dr. Rana Abdelaziz and Dr. Philipp Schulze for their contributions to our own work cited in this review. Thanks are also due to Jenny Lauschke and Laura Schwarz for their assistance with this project during a research internship. We acknowledge funding from the Deutsche Forschungsgemeinschaft (DFG, German Research Foundation) – project number 432291016 (to A.R.) and Mukoviszidose Institut gGmbH (Bonn, Germany), the research and development arm of the German Cystic Fibrosis Association Mukoviszidose e. V. – project number 2202 (to A. R.). Open Access funding enabled and organized by Projekt DEAL.

Conflict of Interests

The authors declare no conflict of interest.

Data Availability Statement

Data sharing is not applicable to this article as no new data were created or analyzed in this study.

Keywords: amino acids · amides · biological activity · antibiotics · drug discovery

[1] *Global Tuberculosis Report 2022*, World Health Organization, Geneva, Switzerland, **2023**.
[2] A. Sharma, M. De Rosa, N. Singla, G. Singh, R. P. Barnwal, A. Pandey, *J. Med. Chem.* **2021**, *64*, 4359–4395.
[3] a) V. N. Dahl, M. Molhave, A. Floe, J. van Ingen, T. Schön, T. Lillebaek, A. B. Andersen, C. Wejse, *Int. J. Infect. Dis.* **2022**, *125*, 120–131; b) I. Ahmed, S. Tiberi, J. Farooqi, K. Jabeen, D. Yeboah-Manu, G. B. Migliori, R. Hasan, *Int. J. Infect. Dis.* **2020**, *92*, S46–S50.
[4] a) T. Baird, S. Bell, *Clinics in Chest Medicine* **2023**, *44*, 847–860; b) A. Gramegna, S. Misuraca, A. Lombardi, C. Premuda, I. Barone, M. Ori, F. Amati, M. Retucci, E. Nazzari, G. Alicandro, M. Ferrarese, L. Codecasa, A. Bandera, S. Aliberti, V. Dacco, F. Blasi, *Respir. Res.* **2023**, *24*, 316.
[5] P. J. McShane, *Clin. Chest Med.* **2023**, *44*, 731–742.
[6] M. R. Loebinger, J. K. Quint, R. van der Laan, M. Obradovic, R. Chawla, A. Kishore, J. van Ingen, *Chest* **2023**, doi:10.1016/j.chest.2023.1006.1014.
[7] D. R. Prevots, J. E. Marshall, D. Wagner, K. Morimoto, *Clin. Chest. Med.* **2023**, *44*, 675–721.
[8] a) Y. M. Boudehen, L. Kremer, *Trends Microbiol.* **2021**, *29*, 951–952; b) M. D. Johansen, J. L. Herrmann, L. Kremer, *Nat. Rev. Microbiol.* **2020**, *18*, 392–407; c) L. Victoria, A. Gupta, J. L. Gomez, J. Robledo, *Front. Cell. Infect. Microbiol.* **2021**, *11*, 659997; d) R. C. Lopeman, J. Harrison, M. Desai, J. A. G. Cox, *Microorganisms* **2019**, *7*; e) K. To, R. Cao, A. Yegiazaryan, J. Owens, V. Venketaraman, *J. Clin. Med.* **2020**, *9*, 2541.
[9] E. S. Saba, G. Ansari, J. Hoerter, L. Schloegel, S. Zim, *Am. J. Otolaryngol.* **2024**, *45*, 104030.
[10] a) E. Marion, L. Marsollier, *Trends Microbiol.* **2022**, *30*, 1116–1117; b) K. Strobel, C. Sickenberger, C. Schoen, H. Kneitz, A. Kolb-Maurer, M. Goebeler, *J. Dtsch. Dermatol. Ges.* **2022**, *20*, 1211–1219.
[11] J. Bhanushali, U. Jadhav, B. Ghewade, P. Wagh, *Cureus* **2023**, *15*, e48270.
[12] a) J. Larkins-Ford, B. B. Aldridge, *Expert Opin. Drug Discovery* **2022**, *18*, 83–97; b) I. Motta, M. Boeree, D. Chesov, K. Dheda, G. Gunther, C. R. Horsburgh, Jr., Y. Kherabi, C. Lange, C. Lienhardt, H. M. McIlleron, N. I. Paton, H. R. Stagg, G. Thwaites, Z. Udwadia, R. Van Crevel, G. E. Velasquez, R. J. Wilkinson, L. Guglielmetti, M. *Clin. Microbiol. Infect.* **2023**, doi: 10.1016/j.cmi.2023.07.013.
[13] T. M. Johnson, T. F. Byrd, W. K. Drummond, L. M. Childs-Kean, M. V. Mahoney, J. C. Pearson, C. G. Rivera, *Infect. Dis. Ther.* **2023**, *12*, 343–365.
[14] T. Greenstein, B. B. Aldridge, *Front. Cell. Infect. Microbiol.* **2023**, *12*, 1085946.
[15] D. Loewenstein, L. van Balveren, A. Lemson, N. Hanemaaijer, W. Hoefsloot, J. van Ingen, *Respir. Med.* **2023**, *217*, 107366.
[16] a) S. H. Kirsch, F. P. J. Haeckl, R. Muller, *Nat. Prod. Rep.* **2022**, *39*, 1226–1263; b) F. Stephanie, U. S. F. Tambunan, T. J. Siahaan, *Life (Basel)* **2022**, *12*, 1774.
[17] a) *WHO consolidated guidelines on tuberculosis. Module 4: treatment - drug-susceptible tuberculosis treatment.*, World Health Organization, Geneva, Switzerland, **2022**; b) M. Grobbelaar, G. E. Louw, S. L. Sampson, P. D. van Helden, P. R. Donald, R. M. Warren, *Infect. Genet. Evol.* **2019**, *74*, 103937.
[18] P. Sensi, *Rev. Infect. Dis.* **1983**, *5*, S402–S406.
[19] a) T. Maitre, A. Baulard, A. Aubry, N. Veziris, *Infect. Dis. Now* **2023**, *54*, 104807; b) R. S. K. Sachan, V. Mistry, M. Dholaria, A. Rana, I. Devgon, I. Ali, J. Iqbal, S. M. Eldin, A. R. Mohammad Said Al-Tawaha, S. Bawazeer, J. Dutta, A. Karnwal, *ACS Omega* **2023**, *8*, 32244–32257.
[20] a) B. R. Imperiale, A. B. Di Giulio, A. Adrian Cataldi, N. S. Morcillo, *J. Antibiot. (Tokyo)* **2014**, *67*, 749–754; b) M. C. Li, X. Y. Wang, T. Y. Xiao, S. Q. Lin, H. C. Liu, C. Qian, D. Xu, G. L. Li, X. Q. Zhao, Z. G. Liu, L. L. Zhao, K. L. Wan, *Infect. Drug. Resist.* **2022**, *15*, 6853–6861; c) M. R. Farhat, J. Sixsmith, R. Calderon, N. D. Hicks, S. M. Fortune, M. Murray, *J. Antimicrob. Chemother.* **2019**, *74*, 1477–1483.
[21] a) C. L. Daley, J. M. Iaccarino, C. Lange, E. Cambau, R. J. Wallace, Jr., C. Andrejak, E. C. Bottger, J. Brozek, D. E. Griffith, L. Guglielmetti, G. A. Huitt, S. L. Knight, P. Leitman, T. K. Marras, K. N. Olivier, M. Santin, J. E. Stout, E. Tortoli, J. van Ingen, D. Wagner, K. L. Winthrop, *Eur. Respir. J.*

2020, *56*; b) M. Yan, S. K. Brode, T. K. Marras, *Clin. Chest. Med.* **2023**, *44*, 799–813.
[22] M. H. Nguyen, C. L. Daley, *Clin. Chest. Med.* **2023**, *44*, 771–783.
[23] U. S. Ganapathy, V. Dartois, T. Dick, *Expert Opin. Drug Discovery* **2019**, *14*, 867–878.
[24] M. R. Holt, T. Baird, *Clin. Chest. Med.* **2023**, *44*, 785–798.
[25] R. A. Adams, G. Leon, N. M. Miller, S. P. Reyes, C. H. Thantrong, A. M. Thokkadam, A. S. Lemma, D. M. Sivaloganathan, X. Wan, M. P. Brynildsen, *J. Antibiot. (Tokyo)* **2021**, *74*, 786–798.
[26] L. Ballell, R. H. Bates, R. J. Young, D. Alvarez-Gomez, E. Alvarez-Ruiz, V. Barroso, D. Blanco, B. Crespo, J. Escribano, R. Gonzalez, S. Lozano, S. Huss, A. Santos-Villarejo, J. J. Martin-Plaza, A. Mendoza, M. J. Rebollo-Lopez, M. Remuinan-Blanco, J. L. Lavandera, E. Perez-Herran, F. J. Gamo-Benito, J. F. Garcia-Bustos, D. Barros, J. P. Castro, N. Cammack, *ChemMedChem* **2013**, *8*, 313–321.
[27] a) J. L. Low, M.-L. Wu, D. B. Aziz, B. Laleu, T. Dick, *Front. Microbiol.* **2017**, *8*; b) A. Richter, A. Strauch, J. Chao, M. Ko, Y. Av-Gay, *Antimicrob. Agents Chemother.* **2018**, *62*, e00828–00818; c) J. Jeong, G. Kim, C. Moon, H. J. Kim, T. H. Kim, J. Jang, *PLoS One* **2018**, *13*, e0195595.
[28] a) W. Lin, S. Mandal, D. Degen, Y. Liu, Y. W. Ebright, S. Li, Y. Feng, Y. Zhang, S. Mandal, Y. Jiang, S. Liu, M. Gigliotti, M. Talaue, N. Connell, K. Das, E. Arnold, R. H. Ebright, *Mol. Cell* **2017**, *66*, 169–179; b) S. Mandal, PhD thesis, Rutgers, The State University of New Jersey (New Brunswick, New Jersey, USA), **2014**.
[29] A. El-Faham, F. Albericio, *Chem. Rev.* **2011**, *111*, 6557–6602.
[30] R. H. Ebright, Y. W. Ebright, S. Mandal, R. Wilde, S. Li, **2015**, *WO2015120320 A1*.
[31] H. Chen, X. Xu, L. L. Liu, G. Tang, Y. Zhao, *RSC Adv.* **2013**, *3*, 16247–16250.
[32] H. Wissmann, H. J. Kleiner, *Angew. Chem. Int. Ed. Engl.* **1980**, *19*, 133–134.
[33] A. A. Waghmare, R. M. Hindupur, H. N. Pati, *Chem. Rev.* **2014**, *4*, 53–131.
[34] L. Mann, M. Lang, P. Schulze, J. H. Halz, R. Csuk, S. Hoenke, R. W. Seidel, A. Richter, *Amino Acids* **2021**, *53*, 1187–1196.
[35] J. Coste, D. Le-Nguyen, B. Castro, *Tetrahedron Lett.* **1990**, *31*, 205–208.
[36] A. Waring, M. M. Joullie, K. M. Lassen, *Arkivoc* **2010**, *2010*, 189–250.
[37] a) D. S. Kemp, J. Rebek, Jr., *J. Am. Chem. Soc.* **1970**, *92*, 5792–5793; b) M. Goodman, L. Levine, *J. Am. Chem. Soc.* **1964**, *86*, 2918–2922.
[38] M. Lang, U. S. Ganapathy, L. Mann, R. Abdelaziz, R. W. Seidel, R. Goddard, I. Sequenzia, S. Hoenke, P. Schulze, W. W. Aragaw, R. Csuk, T. Dick, A. Richter, *J. Med. Chem.* **2023**, *66*, 5079–5098.
[39] M. Lang, U. S. Ganapathy, L. Mann, R. W. Seidel, R. Goddard, F. Erdmann, T. Dick, A. Richter, *ChemMedChem* **2024**, e202300593.
[40] a) H. Li, X. Jiang, Y.-h. Ye, C. Fan, T. Romoff, M. Goodman, *Org. Lett.* **1999**, *1*, 91–94; b) Y. H. Ye, H. Li, X. Jiang, *Biopolymers* **2005**, *80*, 172–178.
[41] F. Li, B. Frett, H.-y. Li, *Synlett* **2014**, *25*, 1403–1408.
[42] G. W. Shipps, Jr., C. C. Cheng, X. Huang, T. O. Fischmann, J. S. Duca, M. Richards, H. Zeng, B. Sun, P. A. Reddy, T. T. Wong, P. K. Tadikonda, M. A. Siddiqui, M. M. Labroli, C. Poker, T. J. Guzi, Schering Corporation, **2008**.
[43] M. Pichette Drapeau, J. Bahri, D. Lichte, L. J. Goossen, *Angew. Chem. Int. Ed. Engl.* **2019**, *58*, 892–896.
[44] P. A. Forero-Cortés, A. M. Haydl, *Org. Process Res. Dev.* **2019**, *23*, 1478–1483.
[45] T. Thiemann, in *Chalcogen Chemistry* (Ed.: P. P. Ndibewu), IntechOpen, Rijeka, **2018**, Ch. 4, doi:10.5772/intechopen.79080..
[46] D. M. Allwood, D. C. Blakemore, A. D. Brown, S. V. Ley, *J. Org. Chem.* **2014**, *79*, 328–338.
[47] O. Santoro, F. Lazreg, Y. Minenkov, L. Cavallo, C. S. Cazin, *Dalton Trans.* **2015**, *44*, 18138–18144.
[48] C. R. Groom, I. J. Bruno, M. P. Lightfoot, S. C. Ward, *Acta Crystallogr. Sect. B* **2016**, *72*, 171–179.
[49] J. Wu, J. Zhang, Y. Jiao, G. Deng, Y. Li, Z. Zhang, Y. Jiang, *J. Org. Chem.* **2021**, *86*, 17462–17470.
[50] J. Bernstein, R. E. Davis, L. Shimoni, N. L. Chang, *Angew. Chem. Int. Ed.* **1995**, *34*, 1555–1573.
[51] M. C. Etter, *Acc. Chem. Res.* **1990**, *23*, 120–126.
[52] T. Garnier, K. Eiglmeier, J.-C. Camus, N. Medina, H. Mansoor, M. Pryor, S. Duthoy, S. Grondin, C. Lacroix, C. Monsempe, S. Simon, B. Harris, R. Atkin, J. Doggett, R. Mayes, L. Keating, P. R. Wheeler, J. Parkhill, B. G. Barrell, S. T. Cole, S. V. Gordon, R. G. Hewinson, *Proc. Natl. Acad. Sci. USA* **2003**, *100*, 7877–7882.
[53] MIC_{90} refers to the compound concentration that inhibits 90% of bacterial growth relative to the untreated control.
[54] M. Esposito, S. Szadocka, G. Degiacomi, B. S. Orena, G. Mori, V. Piano, F. Boldrin, J. Zemanova, S. Huszar, D. Barros, S. Ekins, J. Lelievre, R. Manganelli, A. Mattevi, M. R. Pasca, G. Riccardi, L. Ballell, K. Mikusova, L. R. Chiarelli, *ACS Infect. Dis.* **2017**, *3*, 428–437.
[55] U. S. Ganapathy, T. Dick, *Molecules* **2022**, *27*, 6948.
[56] The factor σ_A is a protein, which is required tio initiate transcription by the mycobacterial RNAP. See, for example: B. Singha, D. Behera, M. Z. Khan, N. K. Singh, D. T. Sowpati, B. Gopal, V. K. Nandicoori, *J. Biol. Chem.* **2023**, *299*, 102933.
[57] A. Mazumder, M. Lin, A. N. Kapanidis, R. H. Ebright, *Proc. Natl. Acad. Sci. USA* **2020**, *117*, 15642–15649.
[58] E. A. Hubin, A. Fay, C. Xu, J. M. Bean, R. M. Saecker, M. S. Glickman, S. A. Darst, E. A. Campbell, *eLife* **2017**, *6*, e22520.
[59] E. A. Campbell, N. Korzheva, A. Mustaev, K. Murakami, S. Nair, A. Goldfarb, S. A. Darst, *Cell* **2001**, *104*, 901–912.
[60] L. Mann, U. S. Ganapathy, R. Abdelaziz, M. Lang, M. D. Zimmerman, V. Dartois, T. Dick, A. Richter, *Microbiol. Spectr.* **2022**, *10*, e0276022.
[61] A. Richter, I. Rudolph, U. Möllmann, K. Voigt, C.-w. Chung, O. M. P. Singh, M. Rees, A. Mendoza-Losana, R. Bates, L. Ballell, S. Batt, N. Veerapen, K. Fütterer, G. Besra, P. Imming, A. Argyrou, *Sci. Rep.* **2018**, *8*, 13473.
[62] S. B. Lakshminarayana, T. B. Huat, P. C. Ho, U. H. Manjunatha, V. Dartois, T. Dick, S. P. Rao, *J. Antimicrob. Chemother.* **2015**, *70*, 857–867.
[63] L. Yu, H. Wan, J. Shi, B. Zhang, M. Wang, *BMC Infect. Dis.* **2023**, *23*, 769.
[64] M. Yee, D. Klinzing, J. R. Wei, M. Gengenbacher, E. J. Rubin, T. Dick, *Genome Announc.* **2017**, *5*, e00388–17.
[65] a) M.-R. Lee, W.-H. Sheng, C.-C. Hung, C.-J. Yu, L.-N. Lee, P.-R. Hsueh, *Emerging Infect. Dis.* **2015**, *21*, 1638–1646; b) L. Strnad, K. L. Winthrop, *Semin. Respir. Crit. Care Med.* **2018**, *39*, 362–376.
[66] U. S. Ganapathy, T. Lan, V. Dartois, C. C. Aldrich, T. Dick, *Microbiol. Spectr.* **2023**, *11*, e01900–01923.
[67] F. P. Maurer, V. L. Bruderer, C. Ritter, C. Castelberg, G. V. Bloemberg, E. C. Bottger, *Antimicrob. Agents Chemother.* **2014**, *58*, 3828–3836.
[68] M. E. Levison, *Infect. Dis. Clin. N. Am.* **2004**, *18*, 451–465.
[69] Q. Chai, L. Wang, C. H. Liu, B. Ge, *Cell Mol Immunol* **2020**, *17*, 901–913.
[70] R. Greendyke, T. F. Byrd, *Antimicrob. Agents Chemother.* **2008**, *52*, 2019–2026.
[71] F. Sorrentino, R. Gonzalez del Rio, X. Zheng, J. Presa Matilla, P. Torres Gomez, M. Martinez Hoyos, M. E. Perez Herran, A. Mendoza Losana, Y. Av-Gay, *Antimicrob. Agents Chemother.* **2016**, *60*, 640–645.
[72] A. Richter, T. Shapira, Y. Av-Gay, *Antimicrob. Agents Chemother.* **2019**, *64*.
[73] K. A. Nash, B. A. Brown-Elliott, R. J. Wallace, Jr., *Antimicrob. Agents Chemother.* **2009**, *53*, 1367–1376.
[74] D. B. Aziz, M. L. Go, T. Dick, *Antibiotics* **2020**, *9*, 72.
[75] C. L. Dulberger, E. J. Rubin, C. C. Boutte, *Nat. Rev. Microbiol.* **2020**, *18*, 47–59.
[76] C. A. Lipinski, *Drug Discovery Today Technol.* **2004**, *1*, 337–341.
[77] J. A. Barrett, W. Yang, S. M. Skolnik, L. M. Belliveau, K. M. Patros, *Drug Discovery Today* **2022**, *27*, 1315–1325.
[78] A. S. Surur, L. Schulig, A. Link, *Arch. Pharm.* **2019**, *352*, e1800248.
[79] S. Kralj, M. Jukič, U. Bren, *Encyclopedia* **2023**, *3*, 501–511.
[80] Medicines for Malaria Venture, www.mmv.org/mmv-open/pathogen-box/about-pathogen-box#composition (accessed on 28 January 2024).
[81] J. Williams, V. Siramshetty, T. Nguyen Eth, E. C. Padilha, M. Kabir, K. R. Yu, A. Q. Wang, T. Zhao, M. Itkin, P. Shinn, E. A. Mathe, X. Xu, P. Shah, *Bioorg. Med. Chem.* **2022**, *56*, 116588.
[82] K. Wanat, *Mol. Biol. Rep.* **2020**, *47*, 3221–3231.
[83] H. Sun, Y. Wang, D. M. Cheff, M. D. Hall, M. Shen, *Bioorg. Med. Chem.* **2020**, *28*, 115422.
[84] B. Ildikó, N. Dániel, F. Ferenc, V. Judit, V. Gábor, F. Pálma, V. Miklós, U. Zoltán, in *Cytotoxicity* (Ed.: Ç. T. Aşkin), IntechOpen, Rijeka, **2017**, Ch. 8, doi: 10.5772/intechopen.72539. .

Manuscript received: January 30, 2024
Accepted manuscript online: April 8, 2024
Version of record online: May 8, 2024